CHEMISTRY
A EUROPEAN JOURNAL

DOI: 10.1002/chem.200601826

Chirality Induction and Protonation-Induced Molecular Motions in Helical Molecular Strands

Elena Kolomiets,[a] Volker Berl,[a, b] and Jean-Marie Lehn*[a]

Abstract: The long oligopyridinedicarboxamide strand **9**, containing 15 heterocyclic rings has been synthesized and its helical structure determined by X-ray crystallography. It was shown that the shorter analogue **6** displays induced circular dichroism and amplification of induced chirality upon dissolution in an optically active solvent, diethyl-L-tartrate. A novel class of helical foldamers was prepared, strands **14**–**16**, based on two oligopyridine carboxamide segments linked through a L-tartaric acid derived spacer. These tartro strands display internal chirality induction as well as chirality amplification. NMR spectroscopy (on **8** and **9**) and circular dichroism (on **16**) studies show that the oligopyridine carboxamide strands undergo reversible unfolding/folding upon protonation. The protonation-induced unfolding has been confirmed by X-ray crystallographic determination of the molecular structure of the extended protonated heptameric form $\mathbf{8}^+$. The molecular-scale mechano-chemical motions of the protonation-induced structural switching consist of a change of the length of the molecule, from 6 Å (**6**, coiled form) to 29 Å ($\mathbf{8}^+$, uncoiled form) for the heptamer and from 12.5 Å (**9**, coiled form, X-ray structure) to 57 Å ($\mathbf{9}^+$, uncoiled form, from modeling) for the pentadecamer. Similar unfolding/folding motional processes take place in the L-tartro strands **15** and **16** upon protonation/deprotonation, with loss of helicity-induced circular dichroism on unfolding as shown for the protonated form $\mathbf{16}^+$.

Keywords: chirality · folding · helical structures · hydrogen bonds · molecular motion

Introduction

The self-organization of molecules into helical and multiple helical architectures can be found throughout nature: from α-helical polypeptides and double-helical nucleic acids to more complex helical protein structures, microtubules, and the protein coating of the tobacco mosaic virus. In the case of the α-helix of polypeptides and the double helix of DNA, hydrogen bonding, stacking interactions, and hydrophobic effects contribute to the formation and stabilization of the helical conformation.[1] The design of nonbiological species that spontaneously organize into helical architectures is of considerable interest in view of their relation to life sciences as well as of their potential applications in materials science, nanotechnology, and optical and electronics devices.[2–9] It requires in particular the identification of *helicity codons*,[3] structural motifs that enforce helical folding of molecular strands.

In synthetic systems, single-helical molecular shapes may be induced through hydrogen bonding,[5,6] conformational preferences,[3,7] solvophobic effects,[8a] cation binding,[8b] and steric interactions.[8c] A family of pyridine-based oligoamide strands was synthesized and studied in our laboratory.[6] Intramolecular hydrogen bonds led to their folding into single-helical conformers, as racemic mixtures of right- and left-handed helices in the solid state as well as in solution.

The transfer of chiral information to achiral or dynamically racemizing molecular, supramolecular, and macromolecular helical systems has attracted great interest in recent years.[9,10] Indeed, chirality transfer can be used for sensing chirality in a wide range of chiral molecules, as well as for developing novel chiroptical devices and chiral materials as enantioselective absorbents and catalysts.[11]

Considerable effort has been focused recently on the development of molecular and supramolecular systems that undergo dynamic structural changes induced by internal or external, physical or chemical triggers. Controlled structural

[a] Dr. E. Kolomiets, Dr. V. Berl, Prof. Dr. J.-M. Lehn
Institut de Science et d'Ingénierie Supramoléculaires (ISIS)
8, allée Gaspard-Monge, BP 70028
67083 Strasbourg cedex (France)
Fax: (+33) 3-9024-5140
E-mail: lehn@isis-ulp.org

[b] Dr. V. Berl
Present address:
ZYMES LLC
777 Terrace Avenue
Hasbrouck Heights, NJ 07604 (USA)

modifications play a most important role in biology, in which they are key to the functioning of motor proteins such as myosin in muscle action, kinesins, and dyneins,[12,13] as well as of rotary motion in the multiprotein ATP synthase assembly.[14–16] Such dynamic processes are of mechanochemical nature, involving chemical reactions like ATP/ADP interconversion, proton transfer, or ion binding. Contraction/extension motions of helical-protein supercoils occur in the bacterial flagellar protofilament,[17] but related artificial systems are rare.

Structural changes of heterocyclic oligomers induced by solvent effects,[18] ion binding,[19] and protonation[20,21] have been described. We recently reported the generation of contraction/extension molecular motion through metal-ion binding and release[19b,c] and by protonation/deprotonation-induced structural switching of pyridine-derived oligoamides between a helical conformation and a protonated linear one.[21]

Herein, we describe the synthesis of new pyridine-based oligoamides, namely the heptameric **6–8** and pentadecameric **9** entities (containing respectively seven and fifteen pyridine groups), that undergo enforced folding into single helices in solution and in the solid state. We also report the induction of chirality in such racemic helical mixtures by external or internal effectors, by using a chiral solvent or a covalently linked chiral tartaric acid fragment, respectively, as in compounds **14–16**.[10]

We finally describe the protonation-induced nanomechanical structural interconversion of such molecular strands between folded and unfolded forms.

Abstract in Russian:

Синтезирован олигопиридиндикарбоксамид **9**, содержащий 15 гетероциклов; его спиралевидная структура была установлена с помощью рентгеноструктурного анализа. Было показано, что более короткий аналог, гептамер **6**, обладает индуцируемым круговым дихроизмом и более выраженной, чем тример **4**, способностью к индукции хиральности при растворении в оптически активном растворителе—диэтил-L-тартрате. Синтезирован новый класс спиралевидных фолдамеров (helical foldamers), состоящих из двух олигопиридинкарбоксамидных сегментов, связанных посредством хирального линкера на основе L-винной кислоты (соединения **14–16**). Эти соединения обнаруживают внутреннюю индукцию хиральности и усиление хиральности при удлинении цепи. Обратимое разрушение вторичной спиралевидной структуры исследуемых соединений при протонировании было обнаружено методом ЯМР (соединения **8** и **9**) и методом кругового дихроизма (соединение **16**), и подтверждено рентгеноструктурным анализом кристаллической структуры развернутой протонированной формы $\mathbf{8}^{+}$. Молекулярные pH-индуцируемые механо-химические движения приводят к значительному изменению длины молекулы при протонировании гептамера—от 6 Å (**6**, скрученная форма) до 29 Å ($\mathbf{8}^{+}$, развернутая форма). Аналогичное явление имеет место также при протонировании/депротонировании соединений **15**, **16**, содержащих линкер L-винной кислоты. На примере протонированной формы $\mathbf{16}^{+}$ показано исчезновение кругового дихроизма, обусловленного спиральностью структуры.

Results and Discussion

Design of the components: Molecular strands such as **6–9**, composed of alternating 2,6-diaminopyridine and 2,6-pyridinedicarbonyl units (Scheme 1), have been found to adopt

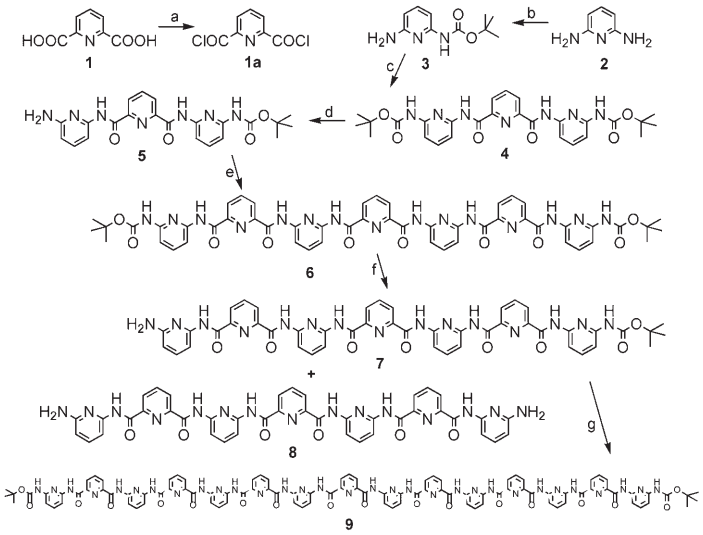

Scheme 1. Synthesis of heptameric and pentadecameric strands: a) $SOCl_2$, reflux; b) Boc_2O, THF, 60 °C, 57 %; c) **1a**, Et_3N, THF, RT, 88 %; d) TMSI, chloroform, RT, then MeOH, reflux, 61 %; e) **1a**, Et_3N, THF, RT, 61 %; f) TMSI, dichloromethane, RT, then MeOH, reflux, 35 %; g) **1a**, Et_3N, THF, RT, 53 %.

a helical conformation both in solution and in the solid state due to the presence of a conformational codon introducing a strong turn (Figure 1).[6] Modeling studies on this codon

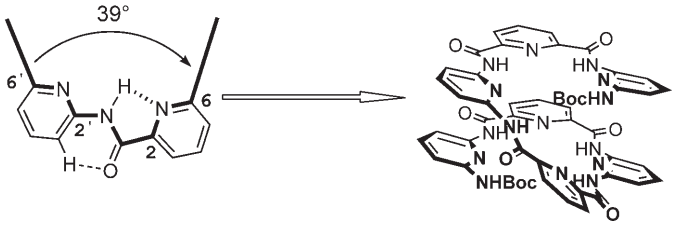

Figure 1. Conformational codon leading to the folding of these oligomers into molecular helices.

suggest that the substituents at the 6- and 6′-positions define an angle of about 39°, deviating substantially from the 60° expected for sp^2 centers with planar trigonal symmetry. As a consequence of this turn, a helical motif forms from strands containing more than five pyridine rings. The heptameric strand was found to undergo a helical folding into 1.6 turns.[6]

The introduction into such oligopyridinedicarboxamide strands of a L-tartaric acid moiety should make it possible to

induce chirality into the helices and obtain an amplification of the molecular chirality. It may also open opportunities for the formation of extended double helical structures.

To this end, the novel chiral foldamer **15** was designed in which two single trimeric strands are connected by a chiral L-tartro spacer. The longer analogue **16** was also synthesized in order to study the influence of the chiral linker on the helical chirality and the amplification of the molecular chirality.

Synthesis: A previously developed monodeprotection strategy[6b] was optimized and applied iteratively to prepare novel heptameric and pentadecameric molecular strands. 2,6-Diaminopyridine (**2**) was efficiently monoprotected by treatment with Boc-anhydride and heating. The monoamine **3** obtained reacted with pyridine-2,6-dicarbonyl dichloride (**1a**) to afford the corresponding bis-Boc-protected trimer **4**. Its monodeprotection was realized by exposure to a stoichiometric amount of TMSI, followed by hydrolysis in methanol, giving the monoamine **5** in 61% yield. This amine was subsequently coupled to **1a** to yield bis-Boc-protected heptamer **6**. After treatment of this compound with a stoichiometric amount of TMSI, followed by hydrolysis in methanol, monoamine **7** and diamine **8** (as a side product) were obtained in 35% and 21% yield, respectively. Monoamine **7** was subsequently coupled to **1a** to yield the bis-Boc-protected pentadecamer **9** (Scheme 1). Despite the lack of alkoxy chains, pentadecamer **9** is still soluble in chlorinated solvents due to the presence of the Boc-protection groups.

For the preparation of the L-tartaric bis-(pyridine-based oligoamide) strands **14**–**16**, a convergent synthetic procedure was applied. Preparative quantities of L-*O*,*O*-didodecyl-tartaric diacid **13**[22] were obtained by *O*-alkylation of *N*,*N*,*N*′,*N*′-tetramethyl-L-tartaramide (**11**), followed by acidic hydrolysis of the obtained diamide **12**. The latter was subsequently treated with phosphorus pentachloride to give the dichloride **13b**.

Synthesis of the L-tartaric bis-(pyridine-based oligoamide) **14** (Scheme 2) was achieved by statistical acylation of 2,6-diaminopyridine (**2**) with butyryl chloride to yield the monoamide **10**, which was then coupled with **13b**, affording **14** in 42% yield.

Longer strands of L-tartaric bis-(pyridine-based oligoamide) were obtained by coupling the previously prepared monoamines **5** and **7**[6b] with diacid chloride **13b** to yield L-tartaric bis-trimer **15** and L-tartaric bis-heptamer **16**, respectively (Scheme 2).

Compounds **14**–**16** have NMR (^{1}H, ^{13}C) and mass spectral data in agreement with their structure (see Figure 4 and Experimental Section).

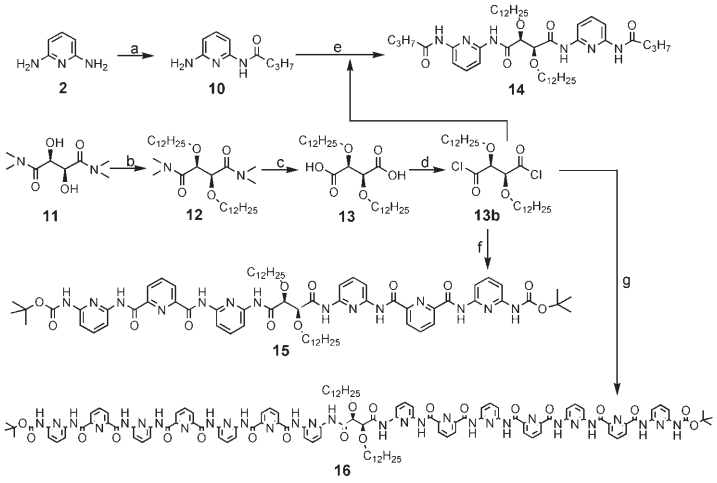

Scheme 2. Synthesis of strands **14**–**16**: a) butyryl chloride, Et_3N, THF, 0°C, 60%; b) dodecyl iodide, NaH, DMF, 80°C, 40%; c) conc. HCl/H_2O, reflux, 68%; d) PCl_5, Et_2O, RT; e) Et_3N, THF, RT, 42%; f) **5**, Et_3N, THF, RT, 40%; g) **7**, Et_3N, THF, RT, 38%.

Helicity of the molecular strands

*Formation of a single helix by the pentadecamer **9** in the solid state*: The pentadecamer **9** is highly crystalline. A single crystal of **9** was obtained by liquid/liquid diffusion and was analyzed by X-ray diffraction. In the crystal, pentadecamer **9** adopts a single-helix conformation presenting three helical turns in accordance with the previous structures determined for the penta-, hepta-, and undecamer[6a,b] (Figure 2).

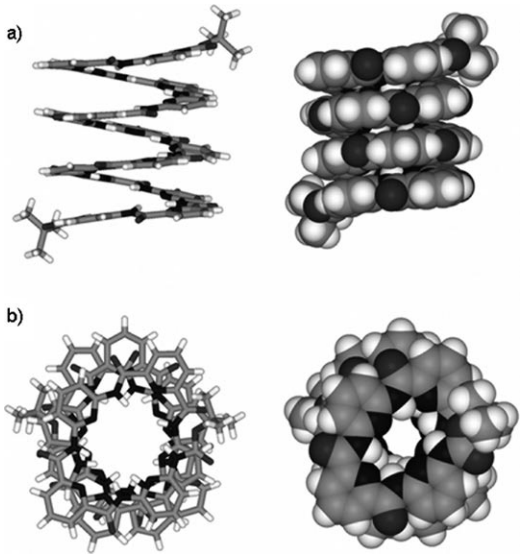

Figure 2. Cylindrical bonds (left) and CPK representations (right) of the solid-state molecular structure of the single helix formed by pentadecamer **9**, determined by X-ray crystallography: a) side view; b) top view.

Within pyridinecarboxamide groups, intramolecular hydrogen bonds form between the hydrogen atoms of the amide groups and the pyridine nitrogen atom with typical distances of 2.21–2.24 Å (Figure 1).

In the crystal structure of pentadecamer **9**, the aromatic ring n overlaps with the aromatic ring $n+4$. The helical pitch (the distance along the helix axis between ring n and

ring $n+4$) is 3.5 Å. This indicates a tight Van der Waals contact between aromatic rings, suggesting that stacking likely plays a role in the cohesion of the structure. The helix of pentadecamer **9** and its central void have a slightly elliptical shape (Figure 2b). The axes of the helix are 13.48 and 10.82 Å long, those of the internal voids are 8.17 and 5.55 Å long. The internal cavity contains several water molecules, probably forming hydrogen bonds with the strand.

Table 1 gives a comparative presentation of the helical structure of **9** and the previously determined structure of the shorter analogue **6**.

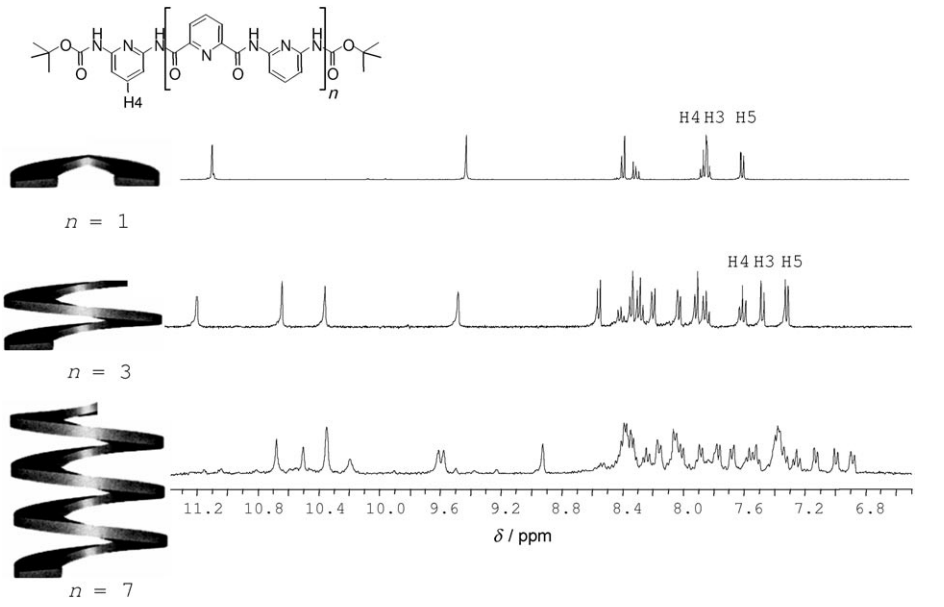

Figure 3. Part of the 400 MHz ^{1}H NMR spectra of trimer **4**, heptamer **6** and pentadecamer **9** in [D_6]DMSO at 25 °C.

For a symmetrical helical structure, the line going through the nitrogen atom and the C4 carbon atom of the central pyridine ring should be a C_2-symmetry axis. The helix formed by pentadecamer **9** is indeed perfectly C_2 symmetrical, and the line going through the nitrogen atom and the C4 carbon atoms of the central pyridine ring is a crystallographic symmetry axis. Thus, the crystallographic asymmetric unit cell contains only half a helix. On the other hand, the helix formed by heptamer **6** deviates slightly from a perfect C_2 symmetry. The series of torsional angles between consecutive pyridine rings at the two strand termini are not identical (Table 1). As a result, the crystallographic unit cell contains an entire strand.

As for the previously determined helical structure of **6**, pentadecamer **9** belongs to a nonchiral space group, which means that plane symmetrical right- and left-handed helical strands are present in the crystal.

*Single-helix formation by strands **6** and **9** in solution*: Dilute solutions of the oligomeric strands **6** and **9** in deuterated chloroform or DMSO feature sharp proton NMR spectra consistent with the presence of a single well-defined species. In all cases, the pattern of the signals indicates that on average, the molecular strands adopt a symmetrical structure with respect to the central pyridine ring. Figure 3 shows the ^{1}H NMR spectra of solutions of trimeric (**4**, $n=1$), heptameric (**6**, $n=3$) and pentadecameric (**9**, $n=7$) strands in [D_6]DMSO, all of which bear terminal Boc-protecting groups. In these compounds, strand curvature generates half, one-and-a-half, and three turns, respectively.

Comparison of the spectrum of heptamer **6** to that of its shorter analogue, trimer **4**, shows that a number of signals are substantially shifted upfield, which suggests intramolecular stacking interactions in **6**. The signals of the terminal diaminopyridine rings have chemical shift values of $\delta=7.48$, 7.32 (H3 and H5) and 7.61 ppm (H4) in **6**, whereas they are at 7.84, 7.60 (H3 and H5) and 7.86 ppm (H4) in **4** (Figure 3).

These data are consistent with a helical structure of heptamer **6** in solution involving an aromatic overlap between the terminal rings and part of the second-to-last rings. Such an overlap corresponds well to the one-and-a-half helical turn observed in the solid state for heptamer **6**.

For pentadecamer **9** in [D_6]DMSO, much larger upfield shifts of the hydrogen-bonded NH protons and of the aromatic signals are observed (Figure 3), which again indicates a helical conformation.

The folding of the strands into helices is enforced by intramolecular hydrogen bonding and further stabilized by aromatic stacking interactions, which are both strong in low polarity solvents, such as chloroform. Two-dimensional NMR studies in deuterated chloroform were carried out in order to reveal contacts between remote atoms that may

Table 1. Characteristics of the helical structures in the solid state.

Compound	Helical pitch	Torsional angles[°] pyridine–pyridine	Outer diameters of elipsoidal cavity [Å][a]	Inner diameters of elipsoidal cavity [Å][b]
6	3.58	6.2, 16.7, 13.7, 8.0, 16.3, 2.3	13.67; 10.98	8.28; 5.58
9	3.50	7.0, 14.2, 11.3, 17.7, 15.2, 15.8, 8.0, 8.0, 15.8, 15.2, 17.7, 11.3, 14.2, 7.0	13.48; 10.82	8.17; 5.55

[a] C–C atom center distances. [b] N–N atom center distances.

come in close proximity upon helix folding. However, NOESY spectra were complicated by correlation signals caused by exchange phenomena resulting from the dimerization of the helices.[6c] Nevertheless, NOESY signals were even observed at low concentration, in which the dimer is present in only minor amounts.

Since the present helical self-organization process leads to the stacking of heteroaromatic pyridine rings of the molecular strands **6** and **9**, spectroscopic examination of intramolecular interactions between these chromophores is of interest.

The excimer formation by heptamer **6** and pentadecamer **9** resulting from the self-organized stacking of the pyridine residues in the helix was revealed by UV/Vis absorption and fluorescence studies and confirmed the helical conformation of these molecular strands.[21]

*Single-helix formation by tartro-strands **14–16** in solution*: Dilute solutions of the molecular strands **14–16** in deuterated chloroform or DMSO show sharp proton NMR spectra consistent with the presence of a single well-defined species. In all cases, the pattern of signals indicates that the molecular strands adopt a symmetrical structure with respect to the tartaric acid derived spacer.

Figure 4 shows the ^{1}H NMR spectra of solutions of **14–16** in deuterated chloroform. From **14** to **15** a strong deshielding of the amide hydrogens is observed due to their participation in the hydrogen bonding that causes the curvature of the strand **15**. From **15** to **16** the shifting of amide hydrogen atoms is related to the hydrogen bonding in the two helically wrapped heptameric type segments of **16**.

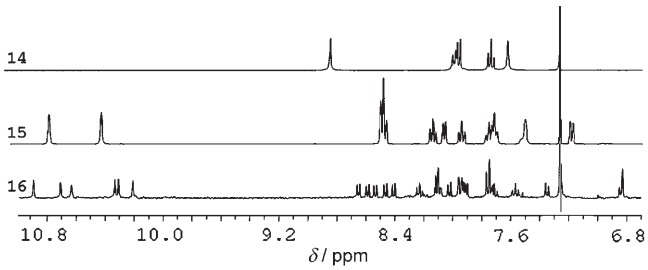

Figure 4. Part of the 400 MHz ^{1}H NMR spectra of molecular strands **14–16** in $CDCl_3$ at 25 °C. For **15** and **16** the signals above 10 ppm correspond to the amide protons between two pyridine groups; the other two NH signals are located in the aromatic region. The spectrum of **15** in DMSO is described in the Experimental Section.

Moreover, two-dimensional NMR studies in deuterated chloroform were carried out in order to reveal NOESY contacts between remote atoms that may come in close proximity upon the formation of a supramolecular architecture by **15** and thus to determine its conformation. NOE signals due to the interactions of terminal amide protons with the asymmetric center-OCH protons, with the ester OCH_2 protons of the tartaric acid derived spacer, and with aromatic protons were observed. These correlation signals are in agreement with the expected helical conformation of **15**.

Unfortunately, no crystals of **15** and its longer analogue **16** were obtained, possibly due to the presence of long alkyl chains. The following UV/Vis absorption, fluorescence, and CD studies further confirm helix formation by **15**.

UV/Vis absorption study: The electronic absorption spectra of the molecular strands **14–16** in chloroform display absorption maxima at 292, 295, and 298 nm respectively, due to π–π* electronic transition of the pyridine moiety (Figure 5). From **14** to **16** a slight red-shift (bathochromic effect) was observed that can be attributed to the increased number of conjugated pyridine rings. The values of the molar absorptivity for the chiral foldamers **14–16** show a hyperchromic effect from **14** to **16** (ε [$M^{-1}cm^{-1}$] = 25000 (**14**), 29000 (**15**), 72000 (**16**)), as expected for an increased number of pyridine rings.

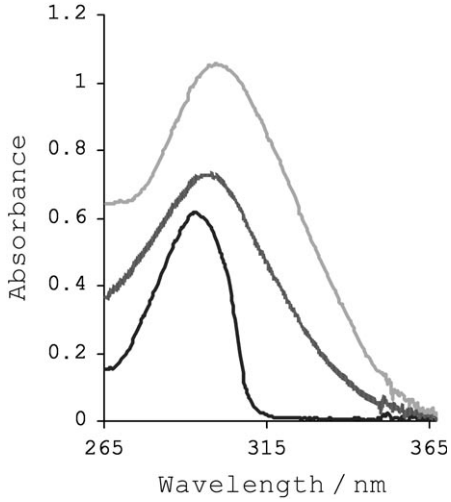

Figure 5. Electronic absorption spectra of the molecular strands **14–16** ($CHCl_3$, 10^{-5} M): **14** (——), **15** (——), **16** (——).

Fluorescence emission study: On excitation of a 10^{-5} M solution of L-tartaric bis-monomer **14** in chloroform at 320 nm, pyridine-like fluorescence is observed at about 363 nm. Excitation of **15** under similar conditions resulted in the observation of a broad band at 437 nm and weak pyridine fluorescence (Figure 6). These hypo- and bathochromic effects observed on going from **14** to **15** can be attributed to the formation of excimers, as it was found for related oligopyridinedicarboxamide helical molecular strands **6** and **9**.[21] These excimers result from the self-organized stacking of the pyridine residues in the helix, thus indicating a helical conformation of **15**.

From L-tartaric bis-trimer **15** to L-tartaric bis-heptamer **16**, a strong increase in fluorescence is observed (hyperchromic effect) due to the increased number of overlapping pyridine rings (Figure 6).

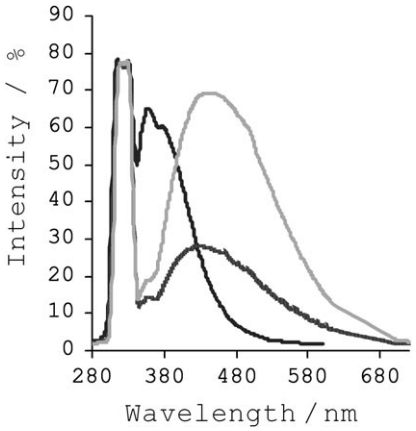

Figure 6. Fluorescence emission spectra of the molecular strands **14**–**16** ($CHCl_3$, 10^{-5} M): **14** (——), **15** (——), **16** (——).

Chirality induction

Induced circular dichroism: Optical activity may be induced in a symmetric substrate when optically active solvents are used for its dissolution.[23] The solvation gives rise to an asymmetric perturbation of the chromophoric substrate that induces a circular dichroism (CD) band in its UV-absorbing region. Such induced CD (ICD) spectra have been observed in a number of situations in which complexation between chiral and achiral partners (host–guest systems) takes place, when the conditions are such that the effect from perturbation can be studied by CD.[10,23]

*Solvent-induced chirality of oligopyridinedicarboxamide molecular strand **6***: The coiled molecular strand **6** may present either right-handed (plus, *P)* or left-handed (minus, *M*) helicity[24] and exists in solution as a racemic (*P*,*M*) mixture of dynamically interconverting *P* and *M* helices. Induction of chirality into such racemic molecular strands was observed under chiral solvation of **4** and **6** dissolved in the optically active solvent L- and D-diethyl tartrate.

Tartaric acid is a chiral species, widely used as a chiral reagent, chiral-resolving agent, and chiral auxiliary in organic synthesis,[23] and it may induce CD in achiral molecules.

To study ICD phenomenon of oligopyridinedicarboxamide molecular strands, enantiomeric derivatives of tartaric acid, such as L- and D-diethyl tartrate, were used as chirality-inducing solvents upon dissolution of achiral heptamer **6**.

Chirality-inducing molecules, such as tartrates, can show significantly different CD bands in different achiral environments. Therefore true ICD due to achiral molecules can only be demonstrated in the spectral region outside the absorption bands of the chiral-inducing molecules. The system diethyl tartrate/pyridine-based oligoamide **6** is well-suited because L- and D-diethyl tartrates show CD bands below 240 nm due to the n–π* transition in the carboxylic group, whereas, as shown above, the absorption band of strand **6** displays maxima at 305 nm due to the π–π* electronic transitions.

As was discussed above, heptamer **6** adopts a helical conformation both in solution and in the solid state. The CD spectrum of heptamer **6** recorded in achiral solvent, such as chloroform, shows no CD signal (curve not shown), as strand **6** is a racemic mixture of both helical conformations (*P*,*M*) formed with equal probability and in dynamic equilibrium.

The ICD spectrum of a 10^{-4} M solution of the achiral heptamer **6** in L-diethyl tartrate shows a negative ICD band in the UV-absorbing region of **6** at 322 nm ($\Delta\varepsilon$ [$M^{-1}cm^{-1}$] = −44.2) due to the π–π* electronic transition of the pyridine moiety (curve L-7, Figure 7a). When D-diethyl tartrate was used as solvent, curve D-7, the mirror image of the curve L-7, was obtained with a positive ICD band at 322 nm ($\Delta\varepsilon$ = 43.8; Figure 7a).

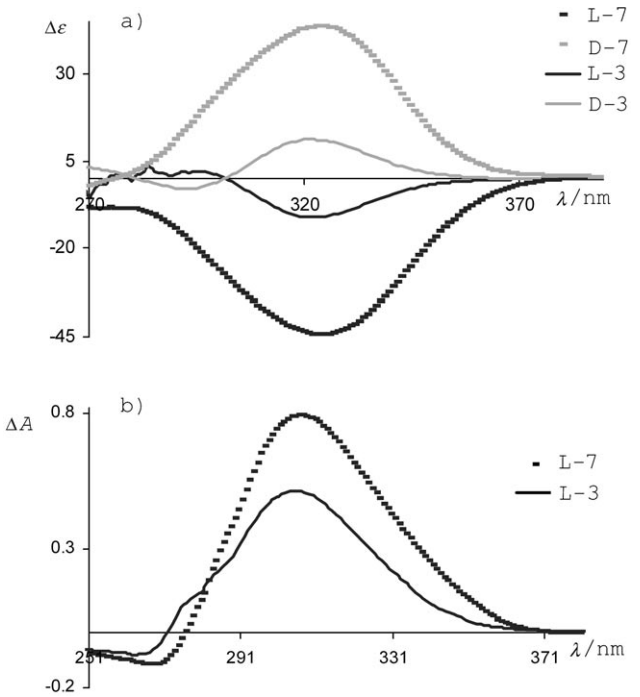

Figure 7. a) Induced circular dichroism (ICD) and b) UV/Vis absorption spectra of 10^{-4} M solutions of achiral trimer **4** (curves L-3 and D-3) and heptamer **6** (curves L-7 and D-7) in L- and D-diethyl tartrate.

The observed phenomena result from the effect of chiral enantiomeric solvents, like L- and D-diethyl tartrate, which, in addition to inducing an asymmetric perturbation of transition moments, may perturb the equilibrium between the right- and left-handed helical conformations of **6**, causing a preference for one helical sense and thus giving negative or positive ICD band, as illustrated in Figure 8.

*Amplification of induced chirality by helical heptamer **6***: The ICD spectra of 10^{-4} M solutions of the achiral trimer **4** in L- and D-diethyl tartrate were recorded (curve L-3 and D-3, respectively, Figure 7a). Comparison of the ICD spectrum of the heptamer **6** to that of its shorter analogue trimer **4** re-

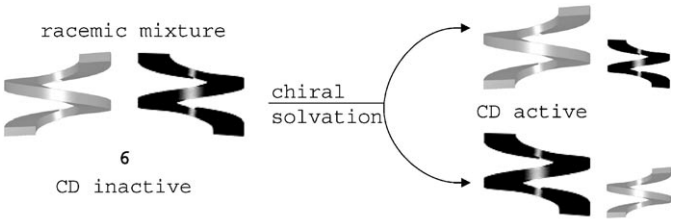

Figure 8. Schematic illustration of the perturbation of the equilibrating *P* and *M* helical forms of heptamer **6** upon dissolution in optically active solvents, such as L- and D-diethyl tartrate.

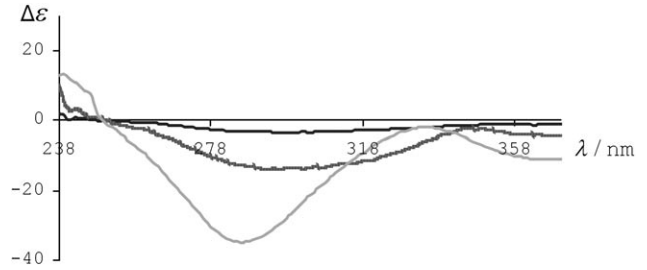

Figure 9. Circular dichroism spectra of 10^{-5} M solutions of the molecular strands **14**–**16** in $CHCl_3$: **14** (——), **15** (——), **16** (——).

corded in D-diethyl tartrate shows that the ICD bands of both molecular strands appear at the same wavelength (322 nm), but that $\Delta\varepsilon$ is much smaller for trimer **4** and equal to 11.0 (Figure 7a). The UV/Vis absorption coefficient ε in L-, D-diethyl tartrate (ε [$M^{-1}cm^{-1}$] = 26000 (**4**), 40000 (**6**); Figure 7b) increases 1.5 times from trimer **4** to heptamer **6**, whereas $\Delta\varepsilon$ increases 4.0 times. This differential increase in ε and $\Delta\varepsilon$ indicates that, in addition to the effect of the increase in ε, the folding of heptamer **6** into a helix in accordance with the previously obtained data leads to an amplification of the induced chirality.

*Chirality features of strands **15** and **16***: The introduction of asymmetric carbon centers into helical structures leads to mixed chirality features combining asymmetry at a center with helicity, as for example in the case of double helicates generated from molecular strands containing asymmetric carbon centers.[25]

The strands **15** and **16** display interesting additional chirality features due to the simultaneous presence of the asymmetric carbon centers of the tartaric and spacer and of the two oligopyridine dicarboxamide segments that may adopt independently either *P* or *M* helicity:

1) Helical enantiomerism (*P*,*P* and *M*,*M*) and diastereoisomerism (*M*,*P*) depending on whether the two helical segments are of same or opposite helicity.
2) Mixed chirality combining center asymmetry and helicity.
3) Helicity induction by the asymmetric carbon centers into the helical segments that are in dynamic equilibrium between *P* and *M* forms; as the two asymmetric carbon atoms in the L-tartaric acid derived spacer have the same chirality, one expects that the same helicity will be induced into each helical segment, whereas the helicities would be opposite for a *meso*-tartaric spacer.

*Chirality amplification by helical folding of **15***: Circular dichroism (CD) spectra of 10^{-5} M solutions of chiral compounds **14**–**16** were recorded in chloroform. As shown in Figure 9, L-tartaric bis-monomer **14** gives a negative CD band in its UV-absorbing region at 300 nm ($|\Delta\varepsilon| = 3.6$) due to the π–π^* electronic transition of the pyridine moiety. Its longer analogue L-tartaric bis-trimer **15** also gives a negative CD band at the same wavelength region as **14** (295 nm), but $|\Delta\varepsilon|$ is much larger and equal to 13.8. This increase in the molar CD ($\Delta\varepsilon$) by a factor of 3.8 from **14** to **15** is much larger than the increase in UV/Vis absorption coefficient ε (factor of 1.2 from **14** to **15**).

Thus, the amplification of the CD spectrum from **14** to **15** is caused not only by the increase in ε related to the number of pyridine rings, but also by the presence of helical segments in bis-trimer **15**.

Comparison of the spectra of UV/Vis absorption and CD studies of the L-tartaric bis-heptamer **16** to that of its shorter analogue **15** shows that from **15** to **16**, both ε and $\Delta\varepsilon$ increase 2.5 times. The amplification of the CD spectrum from **15** to **16** can then be attributed to the increase in the number of pyridine rings.

In conclusion, chiral information of a tartaric acid derived spacer covalently linked to pyridine-based oligoamide segments is transferred into these strands and amplified due to the helical features of **15** and **16**. This result may be taken to indicate that the helical folding of the oligopyridinecarboxamide segments of **15** and the perturbation of their *P*,*M* equilibrium towards one helicity result in a marked amplification of the optical activity.

Protonation-induced molecular motion in strands 8 and 9: The preferred conformation of the 2,6-diaminocarbonylpyridine group in the coiled strands **4**–**9** have the N–H, and C=O bonds in *syn* and *anti* orientations, respectively, with respect to the direction of the nitrogen lone pair of the pyridine group.[6b,26] Protonation of the latter may be expected to cause a conformational inversion, so as to allow formation of new hydrogen bonds between the carbonyl groups and the pyridinium proton (Figure 10).

In the molecular strands **4**–**9**, protonation may be expected to occur regioselectively at the more basic pyridine nitrogen atoms of the 2,6-diaminopyridine moieties, while the 2,6-pyridinedicarbonyl fragments remain unprotonated. As a result, pronounced shape modifications may occur in these

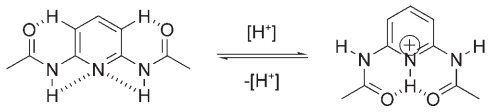

Figure 10. Conformational changes induced by protonation/deprotonation of a 2,6-diaminocarbonylpyridine unit.

strands. Thus, one and two-dimensional NMR experiments were carried out to study the protonation-induced conformational changes of oligoamides **8** and **9**.

Proton NMR investigations: When a suspension of heptamer **8** or pentadecamer **9** in deuterated acetonitrile was treated with triflic acid (four and eight equivalents, respectively), the corresponding protonated species formed immediately and the compounds dissolved. The results of NMR spectroscopy and mass spectrometry studies were in accordance with the formation of the corresponding tetra- and octa-protonated species $\mathbf{8}^{+}$ and $\mathbf{9}^{+}$.

In the case of the tetra-protonated form of heptamer **8**, the signals of the new pyridinium protons Ha and Hb appeared very unshielded at $\delta = 13.5$ and 17.1 ppm respectively, in agreement with a conformation in which they are also hydrogen bonded to one or two amide carbonyl groups (Figure 11). The broadening of the Ha signal can be attributed to the exchange of Ha proton with amine protons. In the bis-Boc derivative **6** the corresponding Ha signal is sharp.

Two-dimensional NMR experiments showed NOE signals due to the interaction of the three different amide protons Hc, Hd, and He with their corresponding vicinal aromatic protons Hf, Hg, and Hh, respectively (Figure 11).

Upon protonation of pentadecamer **9** by the addition of eight equivalents of triflic acid in deuterated acetonitrile, the signals of the new pyridinium protons Ha and Hb also appeared very unshielded at $\delta = 16.2$–17.3 ppm, indicating an *octa*-protonated form $\mathbf{9}^{+}$ (Figure 12). Two-dimensional NMR measurements also showed NOE signals between the amide protons and the adjacent aromatic protons.

Thus, the data of one- and two-dimensional proton NMR experiments agree with the formation of the protonated species $\mathbf{8}^{+}$ and $\mathbf{9}^{+}$ as unfolded, undulating ribbons, resulting from the conformational reorientation of the 2,6-diaminopyridine groups induced by its protonation and the subsequent rearrangement of the hydrogen-bonding pattern.

Molecular structure of the tetra-protonated form $\mathbf{8}^{+}$ in the solid state: Crystals of the heptameric protonated form $\mathbf{8}^{+}$ were obtained by liquid/liquid diffusion and were analyzed by X-ray diffraction. The structural data confirmed the unfolding of the helical strand **8** to give the extended undulating form shown in Figure 13 for $\mathbf{8}^{+}$. In view of the analogous proton NMR spectroscopic features, an extended shape of similar type may be ascribed to the pentadecameric protonated form $\mathbf{9}^{+}$.

The pyridinium protons on the 2,6-aminodicarbonyl centers form hydrogen bonds with one or two carbonyl groups with distances of 1.90–1.97 Å to the oxygen atoms of the carbonyl groups and distances of 2.64–2.67 Å between the pyridinium nitrogen atom and the oxygen atoms of the carbonyl group. The distances between the oxygen atoms of two carbonyl groups hydrogen bonded to the same pyridinium proton are 2.98 and 3.09 Å.

Within the pyridine-2,6-carboxamide groups, intramolecular hydrogen bonds form between the hydrogen atoms of the amide group and the pyridine nitrogen atom, with distances of 2.21–2.25 Å. The distances between the nitrogen atoms of the amide group and the pyridine nitrogen atom are 2.66–2.70 Å, the same as in a previously determined crystal structure of the helical molecular strand **6** (the derivative of **8**).[6a,b]

The molecular-scale mechanochemical consequence of the protonation-induced structural switching is the change of the length and of the hydrodynamic volume of the molecule. For the heptamer, the length changes from 6 Å (**6**, coiled form X-ray structure) to 29 Å ($\mathbf{8}^{+}$, uncoiled form), and for the pentadecamer, from 12.5 Å (**9**, coiled form, X-ray structure) to 57 Å ($\mathbf{9}^{+}$, uncoiled form, from modeling).

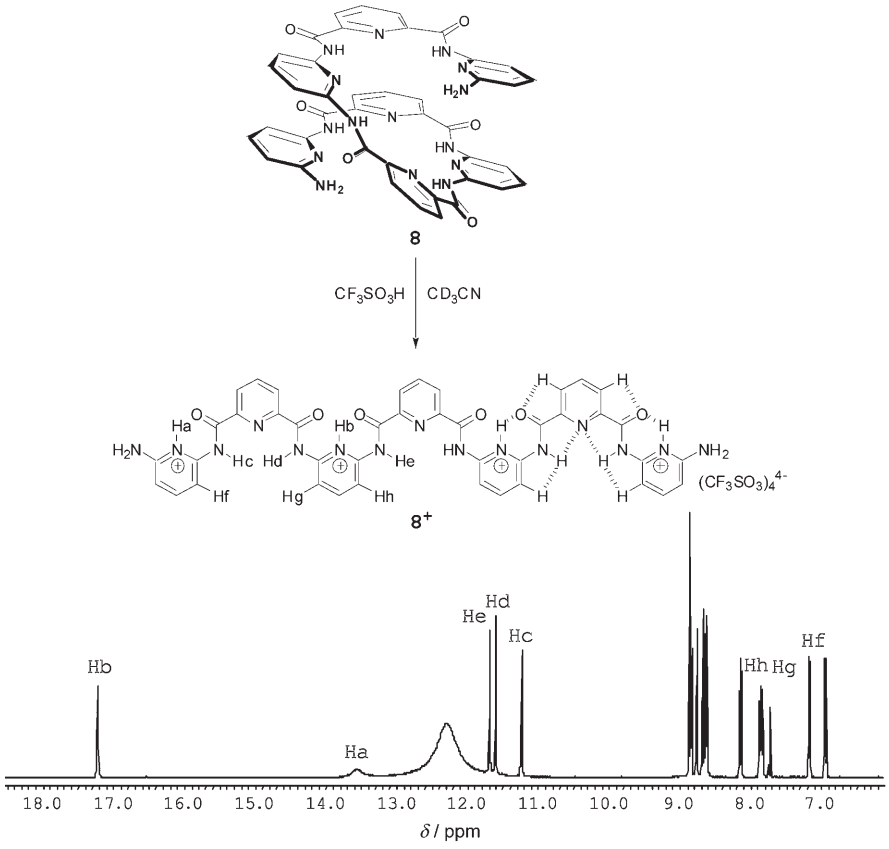

Figure 11. Protonation-induced unfolding of the helical strand **8** to the corresponding extended form $\mathbf{8}^{+}$, and part of the 400 MHz ^{1}H NMR spectrum of the extended form $\mathbf{8}^{+}$ in CD_3CN.

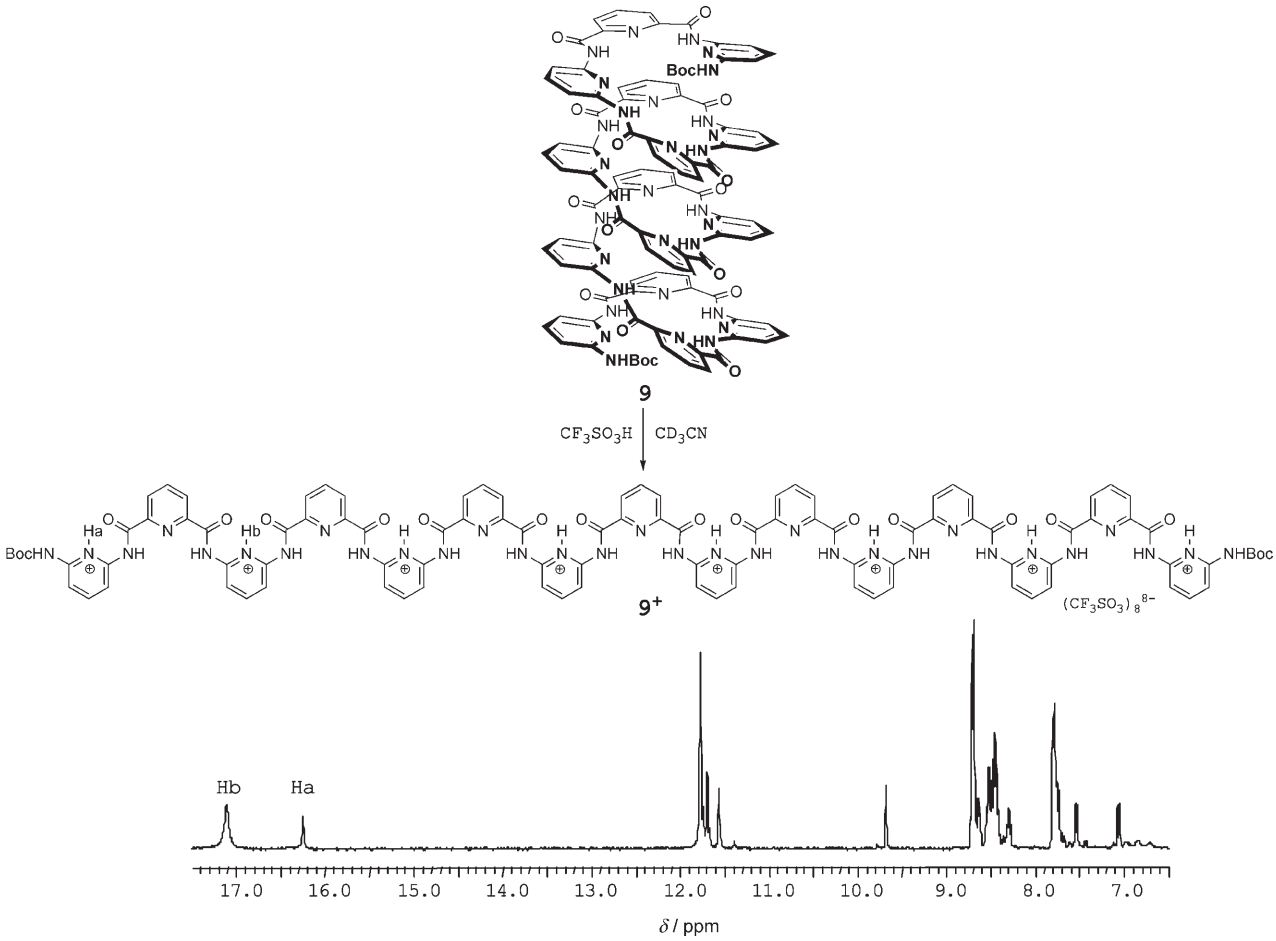

Figure 12. Protonation-induced unfolding of the helical strand **9** to the corresponding extended form $\mathbf{9^+}$, and part of the 400 MHz ^{1}H NMR spectrum of the extended form $\mathbf{9^+}$ in CD_3CN; integration yields Ha (2H) and Hb (6H).

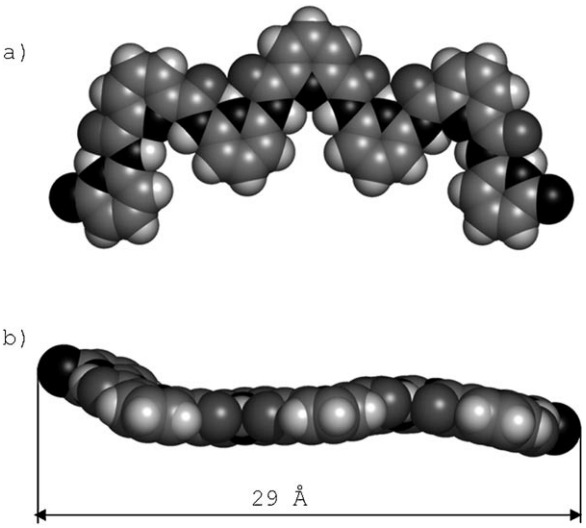

Figure 13. a) Front view and b) side view of the solid-state molecular structure determined for the protonated heptameric form $\mathbf{8^+}$ (triflate anions have been omitted for clarity) by X-ray crystallography. The calculated hydrogen atoms on the terminal NH_2 groups have been omitted.

*Reversible coil–uncoil molecular motion of **8***: The reversibility of the protonation process was corroborated by ^{1}H NMR experiments. As shown in Figure 14, when an excess of triflic acid was added to the heptameric strand **8** in deuterated DMSO a shift of all the signals was observed, showing the formation of unfolded species $\mathbf{8^+}$ (Figure 14b); the signals went back to the starting position after the mixture was treated with an excess of triethylamine, thus indicating the restoring of the initial helicoidal strand **8** (Figure 14c). The broadening of the NH signals may be ascribed to a slow exchange due to the added reagents. The pyridinium protons could not be observed in DMSO, but this solvent was used due to the fact that the heptameric strand **8** is soluble in it, and not in acetonitrile.

Protonation-induced conformational changes in strands 15 and 16: It was shown above that the L-tartaric bis-trimer **15** adopts a helical conformation in solution, which also holds for its longer analogue L-tartaric bis-heptamer **16** in view of the similarity in spectroscopic properties. As these molecular strands may undergo protonation, as described above for **8** and **9**, NMR experiments were carried out to study the

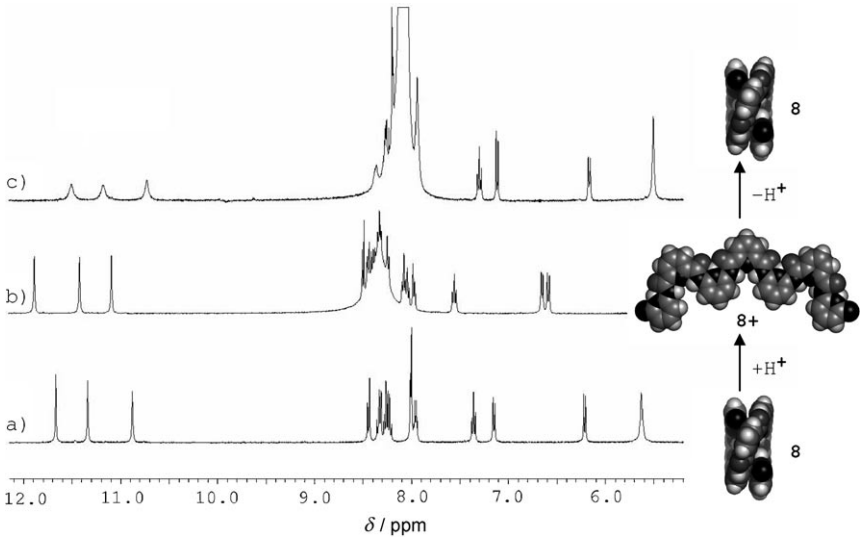

Figure 14. Part of the 400 MHz ^{1}H NMR spectra of a) heptamer **8** in [D$_6$]DMSO, b) after the addition of triflic acid, and c) after addition of an excess of triethylamine. The CPK model of **8** was created based on the crystal structure of **6**.

protonation induced conformational changes of L-tartaric bis-heptamer **16**.

Proton NMR study: When a suspension of bis-heptamer **16** in deuterated acetonitrile was treated with eight equivalents of triflic acid, the corresponding protonated species formed immediately and the compound became soluble. Results of NMR and mass spectrometry studies indicated the formation of the octa-protonated form **16**$^+$ (Figure 15). The signals of the pyridinium protons Ha and Hb appeared very unshielded at $\delta = 16.4$ and 17.1 ppm, respectively, in agreement with a conformation

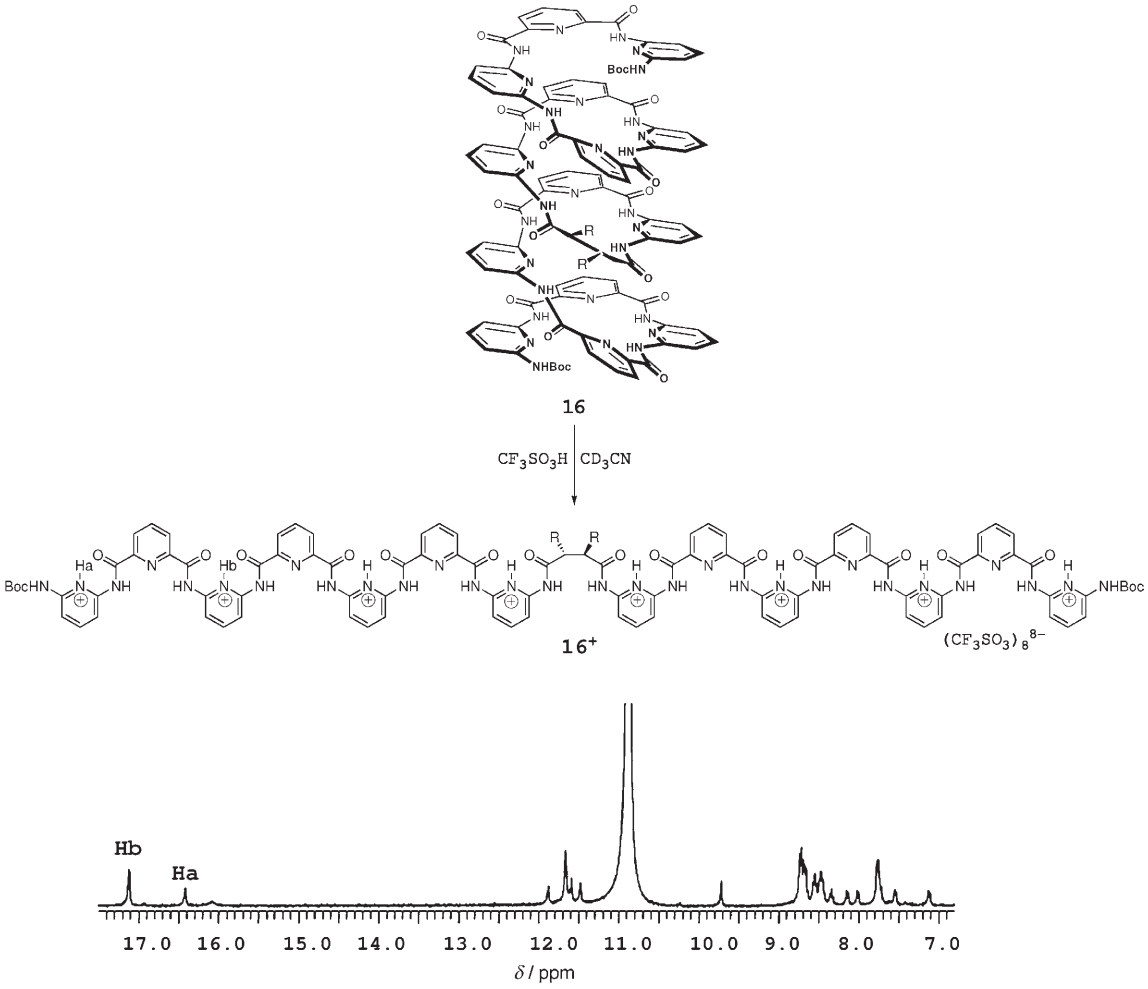

Figure 15. Protonation-induced unfolding of the helical strand **16** to the corresponding extended form **16**$^+$, and part of the 400 MHz ^{1}H NMR spectrum of the extended form **16**$^+$ in CD$_3$CN.

in which they are hydrogen bonded to one or two amide carbonyl groups.

Thus, the NMR data agree with the formation of the protonated form $\mathbf{16}^+$ as unfolded, undulating ribbon, resulting from the conformational reorientation of the 2,6-diaminopyridine groups under protonation, in line with what was found for the related molecular strands **8** and **9**.

Circular dichroism study: Circular dichroism (CD) measurements on the bis-heptamer **16** were performed to corroborate the NMR data. As discussed above, the chiral L-tartaric acid derived spacer of **16** shifts the equilibrium between the right- and left-handed helical conformations of the oligopyridine carboxamide segments, which gives rise to a CD band in the absorption region of the pyridine-based groups associated with its helical conformation. Upon addition of an excess of triflic acid to bis-heptamer **16** in chloroform, this band disappears (Figure 16) as the diaminopyridine units

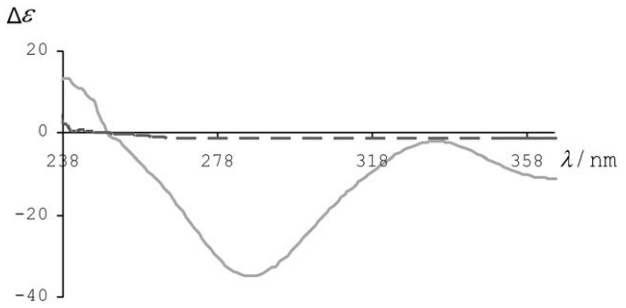

Figure 16. Circular dichroism spectra of 10^{-5} M solutions in $CHCl_3$ of pure bis-heptamer **16** (——)and its corresponding protonated species $\mathbf{16}^+$ (-----) formed under protonation with triflic acid.

are protonated and the nonhelical entity $\mathbf{16}^+$ forms. Subsequent neutralization with an excess of triethylamine restores this CD signal, thus demonstrating the reversibility of the protonation induced conformational changes of **16**. In summary, data of CD experiments are consistent with the proposed transition from the helical conformation to the unfolded extended form for **16**.

Conclusion

The present results extend those previously reported[6] on the helical folding of oligopyridinedicarboxamide strands. In particular, the introduction of a central chiral spacer based on L-tartaric acid gave strands bearing two helically folded oligopyridine-type segments. Furthermore, chiral induction by the asymmetric carbon centers results in helicity induction, with a shift in the equilibrium of the dynamically equilibrating right- and left-handed helices.

Both external (by an optically active solvent) and internal (by asymmetric centers) chirality induction in racemic helical strands and the amplification of molecular chirality by helical folding were revealed for the molecular strands investigated. These molecular strands undergo reversible structural interconversion between helical and extended forms by protonation/deprotonation processes, generating very large amplitude reversible extension/contraction mechano-molecular motions.

In conclusion, the present results corroborate our earlier studies[3,7,26] on the design of *folding codons* based on suitably selected heterocyclic sequences that have well-defined conformational preferences and/or hydrogen-bonding features. Furthermore, they also demonstrate that large amplitude molecular motions may be induced by both reversible ion-binding[19] and protonation processes, fuelled by acid–base neutralization energy.

Experimental Section

General methods: THF was distilled over sodium/benzophenone. Absolute DMF (dried over molecular sieves, $H_2O < 0.005\,\%$) was purchased from Fluka. Triethylamine (Lancaster, 99%) was used as received. 2,6-Diaminopyridine (Aldrich, 98%) was purified by recrystallization from hot chloroform after filtration with charcoal. All other commercially available products were used without further purification. Flash column chromatography was performed using silica gel (Geduran, SI 60; 40–63 μm, Merck). Infrared spectra were recorded as thin films on NaCl discs on a Perkin Elmer 1600 Series FTIR. UV/Vis spectra were recorded on a Varian CARY *3* spectrophotometer. Circular dichroism spectroscopy was performed on a Jasco-810 spectrometer. Fluorescence spectroscopy was performed on an AMINCO-Bowman Series 2 luminescence spectrometer. 400 MHz ^{1}H NMR spectra and 100 MHz ^{13}C NMR spectra were recorded on a Bruker Avance 400 spectrometer, and 200 MHz ^{1}H NMR spectra and 50 MHz ^{13}C NMR spectra on a Bruker SY 200 spectrometer. The solvent signal was used as an internal reference for both ^{1}H and ^{13}C NMR spectra. The following notation is used for the ^{1}H NMR spectral splitting patterns: singlet (s), doublet (d), triplet (t), quartet (q), multiplet (m). Two-dimensional NMR experiments were performed on a Bruker ARX 500 spectrometer and a Bruker Avance 400 spectrometer. FAB-mass spectrometric measurements were performed by the Service de Spectrométrie de Masse, Institut de Chimie, Université Louis Pasteur. Electrospray studies were performed on a Bruker Micro TOF mass spectrometer. Melting points (M.p.) were recorded on a Büchi Melting Point B-540 apparatus and are uncorrected. Elemental analyses were performed by the Service de Microanalyse, Institut de Chimie, Université Louis Pasteur.

X-ray crystallography: X-ray diffraction data for compounds **9** and $\mathbf{8}^+$ were collected on a Nonius KappaCCD diffractometer with a graphite monochromated $Mo_{K\alpha}$ radiation ($\lambda = 0.71071$ Å), phi scans, at 173 K, at the Laboratoire de Cristallochimie, Université Louis Pasteur, Strasbourg. Their structures were determined by Nathalie Kyritsakas and André DeCian using direct methods and refined (based on F^2 using all independent data) by full-matrix least-square methods. Hydrogen atoms were included at calculated positions by using a riding model. The R factors were 8.4 and 16.1% for $\mathbf{8}^+$ and **9**, respectively. The fragility and low diffraction of the crystals of **9** led to a higher *R* factor.

CCDC 220032 ($\mathbf{8}^+$) and CCDC 220031 (**9**) contain the supplementary crystallographic data for this paper. These data can be obtained free of charge from The Cambridge Crystallographic Data Centre via www.ccdc.cam.ac.uk/data_request/cif.

(6-Aminopyridin-2-yl)carbamic acid *tert*-butyl ester (3): A solution of di-*tert*-butyldicarbonate (21.24 g, 97.32 mmol, 100 mol%) in THF (50 mL) was added dropwise to a solution of **2** (10.62 g, 97.32 mmol, 100 mol%) in dry THF (105 mL)at RT. The reaction was allowed to proceed under heating (50–60 °C) for 21 h. Removal of the solvent and purification of the reaction residue by column chromatography (SiO_2; 10% EtOAc/CH_2Cl_2) afforded **3** (11.61 g, 57%) as a white powder. M.p. 125–127.5 °C;

IR (thin film): $\tilde{\nu}$ = 3379, 3211, 2978, 1720, 1619, 1578, 1529, 1457, 1423, 1392, 1368, 1298, 1235, 1158, 1085, 1053, 951, 886, 790, 760, 729 cm^{-1}; ^1H NMR (200 MHz, [D]chloroform): δ = 8.08 (brs, 1H), 7.39 (t, ^3J = 8.0 Hz, 1H), 7.20 (d, ^3J = 8.0 Hz, 1H), 6.14 (d, ^3J = 7.9 Hz, 1H), 4.51 (brs, 2H), 1.50 ppm (s, 9H); ^{13}C NMR (50 MHz, [D]chloroform): δ = 157.3, 152.6, 150.7, 139.8, 102.9, 101.8, 80.8, 28.3 ppm; FAB-MS: *m*/*z* (%): 210.1 (100) $[M+H]^+$; elemental analysis calcd (%) for $C_{10}H_{15}N_3O_2$ (209.24): C 57.40, H 7.23, N 20.08; found: C 57.10, H 7.47, N 19.94.

2,6-Bis-(6-*tert*-butoxycarbonylaminopyridin-2-ylcarbamoyl)pyridine (4): Compound **3** (5.00 g, 23.9 mmol, 200 mol%) and triethylamine (2.66 g, 26.3 mmol, 220 mol%) were dissolved in dry THF (90 mL) and previously prepared diacid chloride **1a** (2.44 g, 12.0 mmol, 100 mol%) in THF (10 mL) was added dropwise at RT. The reaction was allowed to proceed for further 1 h. The reaction mixture was then filtered, evaporated to dryness, and applied to a column of silica (SiO_2; 4% EtOAc/CH_2Cl_2→20% EtOAc/CH_2Cl_2). Compound **4** (5.75 g, 88%) was obtained as a white powder. M.p. 210°C (decomp); IR (thin film): $\tilde{\nu}$ = 3365, 3300, 2979, 2923, 1731, 1696, 1584, 1504, 1461, 1392, 1388, 1297, 1230, 1155, 1074, 1000, 881, 842, 800, 753 cm^{-1}; ^1H NMR (200 MHz, [D_6]DMSO): δ = 11.13 (brs, 2H), 9.45 (brs, 2H), 8.37 (m, 3H), 7.83 (m, 4H), 7.60 (dd, ^3J = 6.4 Hz, ^4J = 2.4 Hz, 2H), 1.43 ppm (s, 18H); ^{13}C NMR (50 MHz, [D_6]DMSO): δ = 162.1, 152.5, 151.0, 149.3, 148.6, 140.0, 139.9, 125.6, 109.5, 109.0, 79.7, 27.9 ppm; FAB-MS: *m*/*z* (%): 550.2 (45) $[M+H]^+$; elemental analysis calcd (%) for $C_{27}H_{31}N_7O_6$ (549.58): C 59.01, H 5.69, N 17.84; found: C 59.19, H 5.78, N 18.00.

(6-{[6-(6-Aminopyridin-2-ylcarbamoyl)pyridine-2-carbonyl]amino}pyridin-2-yl)carbamic acid *tert*-butyl ester (5): TMSI (0.741 g, 0.53 mL, 3.703 mmol, 110 mol%) via a dry syringe was added to compound **4** (1.85 g, 3.366 mmol, 100 mol%) dissolved in chloroform (20 mL) and the mixture was stirred at RT for 30 min. The solvent was then evaporated, the residue was dissolved in methanol (30 mL), and the resulting mixture was heated to reflux for 45 min to hydrolyse the intermediately formed trimethylsilyloxycarbonyl group. After evaporation of the solvent, the solid residue was applied to a column of silica (SiO_2; gradient 10% EtOAc/CH_2Cl_2→30% EtOAc/CH_2Cl_2). Compound **5** (0.92 g, 61%) was obtained as a white powder. M.p. 135–136°C; IR (thin film): $\tilde{\nu}$ = 3366, 3292, 2977, 1730, 1692, 1617, 1582, 1533, 1453, 1392, 1367, 1300, 1233, 1154, 1073, 1001, 884, 793, 748 cm^{-1}; ^1H NMR (200 MHz, [D_6]DMSO): δ = 11.28 (brs, 1H), 11.15 (brs, 1H), 9.53 (brs, 1H), 8.35 (m, 3H), 7.84 (m, 2H), 7.60 (m, 2H), 7.33 (d, ^3J = 7.7 Hz, 1H), 7.42 (d, ^3J = 8.1 Hz, 1H), 1.48 ppm (s, 9H); ^{13}C NMR (50 MHz, [D_6]DMSO): δ = 161.7, 161.2, 157.6, 152.5, 150.6, 148.8, 148.3, 139.7, 139.0, 125.5, 125.3, 108.5, 108.1, 104.6, 102.7, 100.0, 80.3, 27.6 ppm; FAB-MS: *m*/*z* (%): 450.1 (70) $[M+H]^+$; elemental analysis calcd (%) for $C_{22}H_{23}N_7O_4{\cdot}2H_2O$ (449.46): C 54.42, H 5.61, N 20.20; found: C 54.62, H 5.31, N 20.09.

2,6-Bis-(6-{[6-(6-*tert*-butoxycarbonylaminopyridin-2-ylcarbamoyl)pyridine-2-carbonyl]amino}pyridin-2-ylcarbamoyl)pyridine (6): A previously prepared diacid chloride **1a** (0.163 g, 0.59 mmol, 100 mol%) solution in THF (2 mL) was added by means of a cannula to a solution of **5** (0.530 g, 1.18 mmol, 200 mol%) and triethylamine (0.131 g, 1.30 mmol, 220 mol%) in dry THF (30 mL) at RT. The reaction was allowed to proceed for 1 h at RT, at which time **1a** (0.3 equiv) was added to compensate for hydrolyzation. After another 30 min, the reaction mixture was filtered, evaporated to dryness, and subjected to chromatography on a column of silica (SiO_2; 2%EtOH/$CHCl_3$) to afford **6** (0.370 g, 61%) as a white powder. M.p. 280.5–282.5°C; IR (thin film): $\tilde{\nu}$ = 3318, 2971, 1731, 1703, 1582, 1510, 1454, 1392, 1388, 1306, 1229, 1155, 1073, 1002, 800 cm^{-1}; ^1H NMR (200 MHz, [D_6]DMSO): δ = 11.17 (brs, 2H), 10.62 (brs, 2H), 10.34 (brs, 2H), 9.44 (brs, 2H), 8.56 (d, ^3J = 7.8 Hz, 2H), 8.33 (m, 6H), 8.21 (d, ^3J = 6.8 Hz, 2H), 8.02 (d, ^3J = 6.8 Hz, 2H), 7.93 (m, 3H), 7.61 (t, ^3J = 7.8 Hz, 2H), 7.48 (d, ^3J = 7.8 Hz, 2H), 7.31 (d, ^3J = 7.8 Hz, 2H), 1.29 ppm (s, 18H); ^{13}C NMR (50 MHz, [D]chloroform, 65 mM, dimer): δ = 199.1, 160.6, 160.5, 150.9, 149.9, 149.6, 148.7, 147.7, 140.9, 140.4, 140.1, 139.5, 136.7, 125.9, 125.3, 110.1, 109.8, 108.5, 108.1, 107.2, 81.0, 27.8 ppm; FAB-MS: *m*/*z* (%): 1030.3 (65) $[M]^+$), 2060.7 (3) $[M_2]^+$; elemental analysis calcd (%) for $C_{51}H_{47}N_{15}O_{10}$ (1030.01): C 59.47, H 4.60, N 20.40; found: C 59.62, H 4.86, N 20.14.

(6-{[6-(6-{[6-(6-{[6-(6-{[6-(6-Aminopyridin-2-ylcarbamoyl)pyridine-2-carbonyl]-amino}pyridin-2-ylcarbamoyl)pyridine-2-carbonyl]amino}pyridin-2-ylcarbamoyl)pyridine-2-carbonyl]amino}pyridin-2-yl)carbamic acid *tert*-butyl ester (7) and 2,6-bis-(6-{[6-(6-aminopyridin-2-ylcarbamoyl)pyridine-2-carbonyl]amino}pyridin-2-ylcarbamoyl)pyridine (8): TMSI (0.20 g, 0.15 mL, 1.02 mmol, 110 mol%) was added by means of a dry syringe to compound **6** (0.96 g, 0.93 mmol, 100 mol%) dissolved in dichloromethane (100 mL), and the mixture stirred at RT for 2 h. The solvent was then evaporated, the residue was dissolved in methanol (96 mL) and the resulting mixture was heated to reflux for 4 h to hydrolyze the intermediately formed trimethylsilyloxycarbonyl group. After evaporation of the solvent, the solid residue was purified several times by using flash chromatography (SiO_2; 3% EtOH/$CHCl_3$→7% EtOH/$CHCl_3$) to afford **7** (0.30 g, 35%) as a white powder. As a side product of the reaction, compound **8** (0.16 g, 21%) was obtained.

Data for ***7***: M.p. 330°C (decomp); ^1H NMR (400 MHz, [D_6]DMSO): δ = 11.38 (brs, 2H), 11.02 (brs, 2H), 10.73 (brs, 1H), 10.65 (brs, 1H), 9.11 (brs, 1H), 8.47 (d, ^3J = 7.0 Hz, 2H), 8.37–7.91 (m, 13H), 7.65 (t, ^3J = 8.6 Hz, 1H), 7.50 (d, ^3J = 7.8 Hz, 1H), 7.38 (d, ^3J = 8.6 Hz, 1H), 7.29 (t, ^3J = 7.8 Hz, 1H), 7.06 (d, ^3J = 7.8 Hz, 1H), 6.09 (d, ^3J = 8.6 Hz, 1H), 5.53 (brs, 2H), 1.33 ppm (s, 9H); ^{13}C NMR (100 MHz, [D_6]DMSO): δ = 162.2, 162.1, 161.8, 161.2, 161.0, 158.4, 152.0, 150.8, 149.6, 149.0, 148.8, 148.6, 148.5, 148.3, 148.0, 140.4, 140.3, 140.0, 139.9, 139.7, 138.7, 125.7, 125.5, 111.2, 111.0, 110.8, 108.5, 108.3, 104.4, 101.7, 79.5, 27.7 ppm; FAB-MS: *m*/*z* (%): 930.1 (85) $[M+H]^+$; calcd for $C_{46}H_{39}N_{15}O_8$: 929.31; compound **7** was used as intermediate for the synthesis of compound **9**.

Data for ***8***: M.p. 240°C (decomp); ^1H NMR (400 MHz, [D_6]DMSO): δ = 11.65 (brs, 2H), 11.32 (brs, 2H), 10.86 (brs, 2H), 8.43 (d, ^3J = 7.8 Hz, 2H), 8.34–8.21 (m, 8H), 7.99–7.93 (m, 5H), 7.34 (t, ^3J = 7.9 Hz, 2H), 7.13 (d, ^3J = 7.9 Hz, 2H), 6.20 (d, ^3J = 8.2 Hz, 2H), 5.61 ppm (brs, 4H); ^{13}C NMR (100 MHz, [D_6]DMSO): δ = 162.6, 162.3, 161.7, 158.5, 149.9, 149.8, 149.3, 149.0, 148.9, 148.4, 140.5, 139.7, 138.9, 125.9, 125.7, 125.4, 112.2, 111.7, 104.4, 102.2 ppm; FAB-MS: *m*/*z* (%): 830.1 (100) $[M+H]^+$; calcd for $C_{41}H_{31}N_{15}O_6$: 829.26; the structure of compound **8** was confirmed by the crystal structure data (Figure 13).

2,6-Bis-(6-{[6-(6-{[6-(6-{[6-(6-*tert*-butoxycarbonylaminopyridin-2-ylcarbamoyl)-pyridine-2-carbonyl]amino}pyridin-2-ylcarbamoyl)pyridine-2-carbonyl]amino}pyridin-2-ylcarbamoyl)pyridine-2-carbonyl]amino}pyridin-2-ylcarbamoyl)pyridine (9): A previously prepared diacid chloride **1a** (0.037 g, 0.18 mmol, 100 mol%) solution in THF (2 mL) was added by means of a cannula to a solution of **7** (0.34 g, 0.37 mmol, 200 mol%) and triethylamine (0.041 g, 0.40 mmol, 220 mol%) in dry THF (30 mL) at RT The reaction was allowed to proceed for 1 h at RT, at which time **1a** (0.3 equiv) was added to compensate for hydrolyzation. After 2 h, the reaction mixture was filtered, evaporated to dryness and chromatographed on a column of silica (SiO_2; 2%EtOH/$CHCl_3$) to afford **9** (0.19 g, 53%) as a white powder. M.p. 314–314.5°C; ^1H NMR (400 MHz, [D_6]DMSO): δ = 10.31 (brs, 2H), 10.15 (brs, 2H), 10.00 (brs, 4H), 9.87 (brs, 2H), 9.32 (brs, 4H), 8.71 (brs, 2H), 8.21 (m, 9H), 8.09 (t, ^3J = 7.2 Hz, 2H), 8.01 (d, ^3J = 7.2 Hz, 3H), 7.93–7.87 (m, 7H), 7.76 (d, ^3J = 7.2 Hz, 2H), 7.66 (d, ^3J = 7.8 Hz, 2H), 7.57 (d, ^3J = 7.8 Hz, 2H), 7.49–7.41 (m, 4H), 7.30 (m, 6H), 7.19 (t, ^3J = 7.8 Hz, 2H), 7.07 (d, ^3J = 7.9 Hz, 2H), 6.95 (d, ^3J = 8.2 Hz, 2H), 6.85 (d, ^3J = 8.2 Hz, 2H), 1.10 ppm (s, 18H); FAB-MS: *m*/*z* (%): 1991.8 (42) $[M+H]^+$; calcd for $C_{99}H_{79}N_{31}O_{18}$: 1990.62; the structure of compound **9** was confirmed by the crystal structure data (Figure 2).

***N*-(6-Aminopyridin-2-yl)butyramide (10)**: Compound **2** (13.0 g, 119 mmol, 100 mol%) and triethylamine (12.7 g, 119 mmol, 100 mol%) were dissolved in dry THF (200 mL) and the solution cooled to 0°C in an ice bath. A solution of butyryl chloride (12.7 g, 125 mmol, 105 mol%) in THF (20 mL) was added dropwise over a period of 1 h and the reaction allowed to proceed at 0°C for another 3 h, before warming to RT. The reaction mixture was filtered, evaporated to dryness, and subjected to chromatography (SiO_2; gradient: EtOAc/hexane 30:70→60:40). Compound **10** (12.8 g, 60%) was obtained as a white powder. M.p. 154–155.5°C; IR (thin film): $\tilde{\nu}$ = 3326, 3205, 1672, 1620, 1537, 1455, 1294, 1162, 794 cm^{-1}; ^1H NMR (200 MHz, [D_6]DMSO): δ = 9.74 (s, 1H), 7.28 (m, 2H), 6.17 (d, ^3J = 7.2 Hz, 1H), 5.67 (brs, 2H), 2.30 (t, ^3J = 7.1 Hz, 2H), 1.56 (m, 2H), 0.86 ppm (t, ^3J = 7.2 Hz, 3H); ^{13}C NMR (50 MHz,

[D$_6$]DMSO): δ = 171.6, 158.4, 150.5, 138.7, 103.2, 101.0, 38.1, 18.5, 13.5 ppm; FAB-MS: *m*/*z* (%): 180.1 (100) $[M+H]^+$; elemental analysis calcd (%) for $C_9H_{13}N_3O$ (179.22): C 60.32, H 7.31, N 23.45; found: C 60.09, H 7.57, N 23.39.

L-*O*,*O*-Didodecyl-*N*,*N*,*N*′,*N*′-tetramethyltartaramide (12):[28] sodium hydride (60% in oil; 8.23 g, 205.6 mmol, 210 mol%) was suspended in dry DMF (300 mL) under an atmosphere of nitrogen followed by compound **11** (20.0 g, 98.0 mmol, 100 mol%). After another 15 min a solution of dodecyl iodide (60.92 g, 205.6 mmol, 210 mol%) in dry DMF (100 mL) was added dropwise under nitrogen. After stirring at RT for 2 h, the reaction mixture was heated at 80 °C for 2.5 days. The reaction was cooled, concentrated in vacuo, and the residue was partitioned between Et_2O (100 mL) and H_2O (100 mL). The organic extract was dried over Na_2SO_4 and concentrated in vacuo. The mixture was purified by column chromatography (SiO_2; 20% EtOAc/CH_2Cl_2→40% EtOAc/CH_2Cl_2). Compound **12** (21.2 g, 40%) was obtained as a yellowish solid. M.p. 56.5–58 °C; ^{1}H NMR (400 MHz, [D]chloroform): δ = 4.69 (s, 2H), 3.54 (dtd, ^2J = 15.5 Hz, ^3J = 7.1 Hz, ^4J = 2.1 Hz, 4H), 3.17 (s, 6H), 2.92 (s, 6H), 1.56 (m, 4H), 1.25 (m, 36H), 0.88 ppm (t, ^3J = 7.1 Hz, 6H); ^{13}C NMR (100 MHz, [D]chloroform): δ = 169.7, 76.6, 69.8, 37.1, 35.7, 31.8, 29.9, 29.5, 26.0, 22.6, 14.0 ppm; FAB-MS: *m*/*z* (%): 541.7 (100) $[M+H]^+$; HRMS (FAB-MS): *m*/*z* calcd for $[C_{32}H_{64}N_2O_4+H]$: 541.4944; found: 541.4937; elemental analysis calcd (%) for $C_{32}H_{64}N_2O_4$ (540.86): C 71.06, H 11.93, N 5.18; found: C 71.26, H 11.96, N 5.32.

L-2,3-*O*,*O*-didodecyltartaric acid (13):[22,28] Compound **12** (0.83 g, 1.53 mmol, 100 mol%) was dissolved in 67% aqueous solution HCl (20.5 mL) and heated to reflux for 4.5 days. The reaction was cooled to RT and extracted with of $CHCl_3$ (30 mL). The organic extract was dried over Na_2SO_4, concentrated in vacuo and washed with hexane (10 mL). The precipitated product was collected by vacuum filtration and dried to give product **13** (0.52 g, 68%) as a wite solid. M.p. 60–61 °C; ^{1}H NMR (400 MHz, [D]chloroform): δ = 4.38 (s, 2H), 3.71 (dt, ^2J = 9.2 Hz, ^3J = 7.1 Hz, 2H), 3.51 (dt, ^2J = 9.2 Hz, ^3J = 7.1 Hz, 2H), 1.60 (br m, 4H), 1.25 (m, 36H), 0.88 ppm (t, ^3J = 7.1 Hz, 6H); ^{13}C NMR (100 MHz, [D$_4$]methanol): δ = 173.0, 81.0, 73.2, 33.1, 30.6, 27.1, 23.8, 14.5 ppm; FAB-MS: *m*/*z* (%): 485.5 (100) $[M-H]^-$; elemental analysis calcd (%) for $C_{28}H_{54}O_6$ (486.72): C 69.09, H 11.18; found: C 68.58, H 11.69.

L-*O*,*O*-Didodecyl-*N*,*N*′-bis-(6-butyrylaminopyridin-2-yl)tartaramide (14): Phosphorus pentachloride (76.0 mg, 0.365 mmol, 250 mol%) was added to a solution of diacid **13** (71.0 mg, 0.146 mmol, 100 mol%) in dry diethyl ether (2 mL), and the reaction was allowed to proceed at RT for 2 h to afford the crude diacid chloride **13b**, which was immediately transferred by means of a cannula to a previously prepared solution of **10** (65.4 mg, 0.365 mmol, 250 mol%) and triethylamine (0.045 mL, 0.321 mmol, 220 mol%) in dry THF (1.5 mL) at RT. After stirring at RT for 18 h, the reaction mixture was filtered, evaporated to dryness, and subjected to chromatography (SiO_2; gradient: EtOAc/hexane 30:70→50:50). Compound **14** (0.05 g, 42%) was obtained as a yellowish oil. ^{1}H NMR (400 MHz, [D]chloroform): δ = 8.81 (s, 2H; NH), 7.98 (d, ^3J = 8.5 Hz, 2H), 7.94 (d, ^3J = 8.5 Hz, 2H), 7.72 (t, ^3J = 8.5 Hz, 2H), 7.63 (s, 2H; NH), 4.40 (s, 2H), 3.65 (dt, ^2J = 9.2 Hz, ^3J = 7.1 Hz, 2H), 3.46 (dt, ^2J = 9.2 Hz, ^3J = 7.1 Hz, 2H), 2.37 (t, ^3J = 7.7 Hz, 4H), 1.76 (qt, ^3J = 7.7 Hz, 4H), 1.52 (m, 4H), 1.22 (m, 36H), 1.01 (t, ^3J = 7.7 Hz, 6H), 0.86 ppm (t, ^3J = 7.6 Hz, 6H); ^{13}C NMR (100 MHz, [D]chloroform): δ = 171.5, 168.8, 149.9, 148.7, 141.0, 110.1, 109.3, 81.6, 73.7, 39.8, 32.0, 29.7, 29.4, 26.1, 22.8, 18.9, 14.2, 13.8 ppm; ES-MS: *m*/*z* (%): 831.6 (80) $[M+Na]^+$; calcd for $C_{46}H_{76}N_6O_6$+Na: 831.57.

L-*O*,*O*-Didodecyl-*N*,*N*′-bis-(6-{[6-(6-*tert*-butoxycarbonylaminopyridin-2-ylcarbamoyl)pyridine-2-carbonyl]amino}pyridin-2-yl)tartaramide (15): Phosphorus pentachloride (69.5 mg, 0.334 mmol, 250 mol%) was added to a solution of diacid **13** (65.0 mg, 0.133 mmol, 100 mol%) in dry diethyl ether (1.4 mL), and the reaction was allowed to proceed at RT for 2 h to afford the crude diacid chloride **13b**, which was immediately transferred by means of a cannula to a previously prepared solution of **5** (150.0 mg, 0.334 mmol, 250 mol%) and triethylamine (0.041 mL, 0.294 mmol, 220 mol%) in dry THF (3 mL) at RT. After stirring at RT for 23 h, the reaction mixture was filtered, evaporated to dryness, and subjected to chromatography (SiO_2; 20% EtOAc/CH_2Cl_2). Compound **15** (72.1 mg, 40%) was obtained as a yellow oil. ^{1}H NMR (400 MHz, [D$_6$]DMSO): δ = 11.50 (s, 2H; NH), 11.22 (s, 2H; NH), 9.57 (s, 2H; NH), 9.19 (s, 2H; NH), 8.41 (t, ^3J = 7.7 Hz, 4H), 8.32 (d, ^3J = 7.7 Hz, 2H), 7.94 (m, 10H), 7.63 (d, ^3J = 7.7 Hz, 2H), 4.37 (s, 2H), 4.18 (dt, ^2J = 9.2 Hz, ^3J = 7.1 Hz, 2H), 3.67 (dt, ^2J = 9.2 Hz, ^3J = 7.1 Hz, 2H), 1.46 (m, 22H), 1.13 (m, 36H), 0.81 ppm (m, 6H); ^{13}C NMR (100 MHz, [D]chloroform): δ = 171.5, 162.1, 161.5, 152.4, 151.0, 150.7, 149.5, 149.0, 148.6, 143.8, 141.1, 140.9, 140.8, 139.7, 126.2, 117.6, 115.2, 108.9, 81.6, 80.5, 72.8, 32.0, 29.8, 28.5, 26.1, 22.8, 14.2 ppm; ES-MS: *m*/*z* (%): 1275.6 (83) $[M-Boc+Na]^+$; elemental analysis calcd (%) for $C_{72}H_{96}N_{14}O_{12}$ (1349.62): C 64.08, H 7.17; found: C 64.04, H 6.94.

L-*O*,*O*-Didodecyl-*N*,*N*′-bis-(6-{[6-(6-{[6-(6-{[6-(6-{[6-(6-*tert*-butoxycarbonylaminopyridin-2-ylcarbamoyl)pyridine-2-carbonyl]amino}pyridin-2-ylcarbamoyl)pyridine-2-carbonyl]amino}pyridin-2-ylcarbamoyl)pyridine-2-carbonyl]amino}pyridin-2-yl)tartaramide (16): Phosphorus pentachloride (29.0 mg, 0.139 mmol, 250 mol%) was added to a solution of diacid **13** (27.0 mg, 0.055 mmol, 100 mol%) in dry diethyl ether (1 mL), and the reaction was allowed to proceed at RT for 2 h to afford the crude diacid chloride **13b**, which was immediately transferred by means of a cannula to a previously prepared solution of **7** (129.0 mg, 0.139 mmol, 250 mol%) and triethylamine (0.017 mL, 0.122 mmol, 220 mol%) in dry THF (5 mL) at RT. After stirring at RT for 23 h, the reaction mixture was filtered, evaporated to dryness, and subjected to chromatography (SiO_2; 80% EtOAc/CH_2Cl_2). Compound **16** (23.5 mg, 38%) was obtained as a yellow solid. M.p. 293–295.5 °C; ^{1}H NMR (400 MHz, [D]chloroform): δ = 10.91 (s, 2H; NH), 10.72 (s, 2H; NH), 10.64 (s, 2H; NH), 10.34 (s, 2H; NH), 10.31 (s, 2H; NH), 10.22 (s, 2H; NH), 8.65 (d, ^3J = 7.7 Hz, 2H), 8.59 (d, ^3J = 8.5 Hz, 2H), 8.54 (d, ^3J = 7.7 Hz, 2H), 8.47 (d, ^3J = 7.7 Hz, 2H), 8.41 (d, ^3J = 7.7 Hz, 2H), 8.24 (d, ^3J = 7.7 Hz, 2H), 8.10 (m, 8H), 8.03 (d, ^3J = 7.7 Hz, 2H), 7.93 (m, 10H), 7.75 (m, 8H), 7.57 (t, ^3J = 7.7 Hz, 2H), 7.35 (d, ^3J = 7.7 Hz, 2H), 6.83 (s, 2H; NH), 3.96 (s, 2H), 3.52 (dt, ^2J = 9.2 Hz, ^3J = 7.1 Hz, 2H), 3.31 (dt, ^2J = 9.2 Hz, ^3J = 7.1 Hz, 2H), 2.29 (m, 4H), 1.32 (s, 18H), 1.25 (m, 36H), 0.88 ppm (t, ^3J = 7.7 Hz, 6H); ^{13}C NMR (100 MHz, [D]chloroform, 23 mM, aggregates): δ = 170.8, 170.4, 161.7, 161.5, 161.3, 161.1, 160.5, 160.4, 151.7, 151.5, 150.4, 150.1, 149.5, 149.4, 149.1, 148.8, 148.7, 148.5, 148.1, 147.9, 147.6, 147.3, 142.9, 141.3, 140.9, 140.2, 139.9, 139.6, 138.9, 138.4, 126.2, 125.9, 125.2, 117.3, 115.1, 114.5, 110.5, 110.3, 109.5, 108.8, 108.2, 106.7, 81.1, 79.1, 72.5, 32.1, 29.8, 27.9, 25.7, 22.8, 14.3 ppm; ES-MS: *m*/*z* (%): 1155.7 (60) $[M]^{2+}$; elemental analysis calcd (%) for $C_{120}H_{128}N_{30}O_{20}$ (2310.49): C 62.38, H 5.58; found: C 62.53, H 5.47.

Acknowledgement

We thank N. Kyritsakas and A. DeCian for the crystal structure determinations. E.K. thanks the French Ministry of Research for a predoctoral fellowship.

[1] C. Branden, J. Tooze, *Introduction to Protein Structure*, Garland, New York, **1991**.

[2] a) A. E. Rowan, R. J. M. Nolte, *Angew. Chem.* **1998**, *110*, 65; *Angew. Chem. Int. Ed.* **1998**, *37*, 63; b) C. Piguet, G. Bernardinelli, G. Hopfgartner, *Chem. Rev.* **1997**, *97*, 2005; c) D. J. Hill, M. J. Mio, R. B. Prince, T. S. Hughes, J. S. Moore, *Chem. Rev.* **2001**, *101*, 3893; d) S. H. Gellman, *Acc. Chem. Res.* **1998**, *31*, 173.

[3] a) G. S. Hanan, J.-M. Lehn, N. Kyritsakas, J. Fischer, *J. Chem. Soc. Chem. Commun.* **1995**, 765; b) M. Ohkita, J.-M. Lehn, G. Baum, D. Fenske, *Chem. Eur. J.* **1999**, *5*, 3471; c) L. A. Cuccia, J.-M. Lehn, J.-C. Homo, M. Schmutz, *Angew. Chem.* **2000**, *112*, 239; *Angew. Chem. Int. Ed.* **2000**, *39*, 233.

[4] a) D. B. Amabilino, E. Ramos, J.-L. Serrano, J. Veciana, *Adv. Mater.* **1998**, *10*, 1001; b) J. J. L. M. Cornelissen, M. Fisher, N. A. J. M. Sommerdijk, R. J. M. Nolte, *Science* **1998**, *280*, 1427; c) C. A. Slate, D. R. Striplin, J. A. Moss, P. Chen, B. W. Ericsson, T. J. Meyer, *J. Am. Chem. Soc.* **1998**, *120*, 4885.

[5] a) T. Kawamoto, B. S. Hammes, B. Haggerty, G. P. A. Yap, A. L. Rheingold, A. S. Borovik, *J. Am. Chem. Soc.* **1996**, *118*, 285; b) Y. Hamuro, J. S. Geib, A. D. Hamilton, *J. Am. Chem. Soc.* **1997**, *119*, 10587; c) P. I. Arvidsson, N. S. Ryder, H. M. Weiss, G. Gross, O. Kretz, R. Woessner, D. Seebach, *ChemBioChem* **2003**, *4*, 1345; d) R. D. Parra, H. Zeng, J. Zhu, C. Zeng, X. C. Zeng, B. Gong, *Chem. Eur. J.* **2001**, *7*, 4352; e) B. Gong, *Chem. Eur. J.* **2001**, *7*, 4336; f) E. A. Archer, H. Gong, M. J. Krische, *Tetrahedron* **2001**, *57*, 1139; g) I. Huc, *Eur. J. Org. Chem.* **2004**, 17; h) D. Seebach, A. K. Beck, D. J. Bierbaum, *Chem. Biodiversity* **2004**, *1*, 1111; i) I. Huc, *Eur. J. Org. Chem.* **2004**, 17; j) G. Licini, L. J. Prins, P. Scrimin, *Eur. J. Org. Chem.* **2005**, 969.

[6] a) V. Berl, I. Huc, R. G. Khoury, M. J. Krische, J.-M. Lehn, *Nature* **2000**, *407*, 720; b) V. Berl, I. Huc, R. G. Khoury, J.-M. Lehn, *Chem. Eur. J.* **2001**, *7*, 2798; c) V. Berl, I. Huc, R. G. Khoury, J.-M. Lehn, *Chem. Eur. J.* **2001**, *7*, 2810.

[7] a) K. M. Gardinier, R. G. Khoury, J.-M. Lehn, *Chem. Eur. J.* **2000**, *6*, 4124; b) A. Petitjean, L. A. Cuccia, J.-M. Lehn, H. Nierengarten, M. Schmutz, *Angew. Chem.* **2002**, *114*, 1243; *Angew. Chem. Int. Ed.* **2002**, *41*, 1195; c) J.-L. Schmitt, A.-M. Stadler, N. Kyritsakas, J.-M. Lehn, *Helv. Chim. Acta* **2003**, *86*, 1598; d) A. Petitjean, H. Nierengarten, A. van Dorsselaer, J.-M. Lehn, *Angew. Chem.* **2004**, *116*, 3781; *Angew. Chem. Int. Ed.* **2004**, *43*, 3695.

[8] a) J. C. Nelson, J. G. Saven, J. S. Moore, P. G. Wolynes, *Science* **1997**, *277*, 1793; b) R. B. Prince, T. Okada, J. S. Moore, *Angew. Chem.* **1999**, *111*, 245; *Angew. Chem. Int. Ed.* **1999**, *38*, 233; c) K. Kirshenbaum, A. E. Barron, R. A. Goldsmith, E. K. Bradley, K. T. V. Truong, K. A. Dill, F. E. Cohen, R. N. Zuckermann, *Proc. Natl. Acad. Sci. USA* **1998**, *95*, 4303.

[9] a) S. Allenmark, *Chirality* **2003**, *15*, 409; b) J. W. Canary, A. E. Holmes, J. Liu, *Enantiomer* **2001**, *6*, 181; c) H. Tsukube, S. Shinoda, *Chem. Rev.* **2002**, *102*, 2389; d) E. Yashima, Y. Okamoto, *Circular Dichroism: Principles and Applications*, Wiley, New York, **2000**.

[10] For helicity induction in synthetic helical strands, see for instance: a) R. B. Prince, L. Brunsveld, E. W. Meijer, J. S. Moore, *Angew. Chem.* **2000**, *112*, 234; *Angew. Chem. Int. Ed.* **2000**, *39*, 228; b) T. Sanji, N. Kato, M. Kato, M. Tanaka, *Angew. Chem.* **2005**, *117*, 7467; *Angew. Chem. Int. Ed.* **2005**, *44*, 7301; c) C. Dolain, H. Jiang, J.-M. Léger, P. Guionneau, I. Huc, *J. Am. Chem. Soc.* **2005**, *127*, 12943; d) M. Melucci, G. Barbarella, M. Gazzano, M. Cavallini, F. Biscarini, A. Bongini, F. Piccinelli, M. Monari, M. Bandini, A. Umani-Ronchi, P. Biscarini, *Chem. Eur. J.* **2006**, *12*, 7304; e) M. Waki, H. Abe, M. Inouye, *Chem. Eur. J.* **2006**, *12*, 7839; f) T. Sanji, N. Kato, M. Tanaka, *Org. Lett.* **2006**, *8*, 235.

[11] a) Y. Okamoto, T. Nakano, *Chem. Rev.* **1994**, *94*, 349; b) Y. Okamoto, E. Yashima, *Angew. Chem.* **1998**, *110*, 1072; *Angew. Chem. Int. Ed.* **1998**, *37*, 1020.

[12] B. Alberts, D. Bray, J. Lewis, M. Raff, K. Roberts, J. D. Watson, *Molecular Biology of the Cell*, Garland, New York, **1994**.

[13] T. Kreis, R. Vale, *Cytoskeletal and Motor Proteins*, Oxford University Press, Oxford, **1999**.

[14] P. D. Boyer, *Angew. Chem.* **1998**, *110*, 2424; *Angew. Chem. Int. Ed.* **1998**, *37*, 2296.

[15] W. S. Allison, *Acc. Chem. Res.* **1998**, *31*, 819.

[16] J. E. Walker, *Angew. Chem.* **1998**, *110*, 2438; *Angew. Chem. Int. Ed.* **1998**, *37*, 2308.

[17] a) K. Namba, F. Vonderviszt, *Q. Rev. Biophys.* **1997**, *30*, 1; b) F. A. Samatey, K. Imada, S. Nagashima, F. Vonderviszt, T. Kumasaka, M. Yamamoto, K. Namba, *Nature* **2001**, *410*, 331.

[18] D. J. Hill, J. S. Moore, *Proc. Natl. Acad. Sci. USA* **2002**, *99*, 5053.

[19] a) M. Barboiu, J.-M. Lehn, *Proc. Natl. Acad. Sci. USA* **2002**, *99*, 5201; b) A.-M. Stadler, N. Kyritsakas, J.-M. Lehn, *Chem. Commun.* **2004**, 2024.

[20] C. Dolain, V. Maurizot, I. Huc, *Angew. Chem.* **2003**, *115*, 2844; *Angew. Chem. Int. Ed.* **2003**, *42*, 2738.

[21] E. Kolomiets, V. Berl, I. Odriozola, A.-M. Stadler, N. Kyritsakas, J.-M. Lehn, *Chem. Commun.* **2003**, 2868.

[22] C. Fouquey, J.-M. Lehn, A.-M. Levelut, *Adv. Mater.* **1990**, *2*, 254.

[23] a) B. Bosnich, *J. Am. Chem. Soc.* **1966**, *88*, 2606; b) L. D. Hayward, R. N. Totty, *Can. J. Chem.* **1971**, *49*, 624; c) B. Norden, *Chem. Scr.* **1975**, *8*, 20.

[24] For reviews on molecular helicity, see a) J. H. Brewster, *Top. Curr. Chem.* **1974**, *47*, 29.

[25] W. Zarges, J. Hall, J.-M. Lehn, *Helv. Chim. Acta* **1991**, *74*, 1843.

[26] I. Odriozola, N. Kyritsakas, J.-M. Lehn, *Chem. Commun.* **2004**, 62.

[27] a) J. Gawronski, K. Gawronska, *Tartaric and Malic Acids in Synthesis: A Source Book of Building Blocks, Ligands, Auxiliaries, and Resolving Agents*, Wiley-Interscience, New York, **1999**; b) J. Gawronski, J. Grajewski, *Org. Lett.* **2003**, *5*, 3301.

[28] M. J. Krische, A. Petitjean, E. N. Pitsinos, J.-M. Lehn, unpublished results.

Received: December 19, 2006
Published online: April 11, 2007

